

# Transiting exoplanets from the CoRoT space mission<sup>★</sup>

## XX. CoRoT-20b: A very high density, high eccentricity transiting giant planet

M. Deleuil<sup>1</sup>, A.S. Bonomo<sup>1</sup>, S. Ferraz-Mello<sup>11</sup>, A. Erikson<sup>10</sup>, F. Bouchy<sup>4,5</sup>, M. Havel<sup>18</sup>, S. Aigrain<sup>6</sup>, J.-M. Almenara<sup>1</sup>, R. Alonso<sup>17</sup>, M. Auvergne<sup>2</sup>, A. Baglin<sup>2</sup>, P. Barge<sup>1</sup>, P. Bordé<sup>3</sup>, H. Bruntt<sup>20</sup>, J. Cabrera<sup>9</sup>, Sz. Csizmadia<sup>10</sup>, C. Damiani<sup>1</sup>, H.J., Deeg<sup>7,8</sup>, R. Dvorak<sup>9</sup>, M. Fridlund<sup>12</sup>, G. Hébrard<sup>4,5</sup>, D. Gandolfi<sup>12</sup>, M. Gillon<sup>13</sup>, E. Guenther<sup>14</sup>, T. Guillot<sup>18</sup>, A. Hatzes<sup>14</sup>, L. Jorda<sup>1</sup>, A. Léger<sup>3</sup>, H. Lammer<sup>15</sup>, T. Mazeh<sup>16</sup>, C. Moutou, C.<sup>1</sup>, M. Ollivier<sup>3</sup>, A. Ofir<sup>21</sup>, H. Parviainen<sup>7,8</sup>, D. Queloz<sup>17</sup>, H. Rauer<sup>10</sup>, A. Rodríguez<sup>11</sup>, D. Rouan<sup>2</sup>, A. Santerne<sup>1</sup>, J. Schneider<sup>19</sup>, L. Tal-Or<sup>16</sup>, B. Tingley<sup>7,8</sup>, J. Weingrill<sup>??</sup>, and G. Wuchterl<sup>14</sup>

(Affiliations can be found after the references)

Received ; accepted

### ABSTRACT

We report the discovery by the *CoRoT* space mission of a new giant planet, *CoRoT-20b*. The planet has a mass of  $4.24 \pm 0.23 M_{\text{Jup}}$  and a radius of  $0.84 \pm 0.04 R_{\text{Jup}}$ . With a mean density of  $8.87 \pm 1.10 \text{ g cm}^{-3}$ , it is among the most compact planets known so far. Evolution models for the planet suggest a mass of heavy elements of the order of  $800 M_{\oplus}$  if embedded in a central core, requiring a revision either of the planet formation models or of planet evolution and structure models. We note however that smaller amounts of heavy elements are expected from more realistic models in which they are mixed throughout the envelope. The planet orbits a G-type star with an orbital period of 9.24 days and an eccentricity of 0.56. The star's projected rotational velocity is  $v \sin i = 4.5 \pm 1.0 \text{ km s}^{-1}$ , corresponding to a spin period of  $11.5 \pm 3.1$  days if its axis of rotation is perpendicular to the orbital plane. In the framework of Darwinian theories and neglecting stellar magnetic braking, we calculate the tidal evolution of the system and show that *CoRoT-20b* is presently one of the very few Darwin-stable planets that is evolving towards a triple synchronous state with equality of the orbital, planetary and stellar spin periods.

**Key words.** stars: planetary systems - stars: fundamental parameters - techniques: photometry - techniques: radial velocities - techniques: spectroscopy

### 1. Introduction

The existence of a planet population at very short orbital distance,  $a < 0.1 \text{ AU}$  typically, with its wide range of orbital and physical properties is an intriguing phenomenon. In-situ formation of such massive bodies so close to their host-star at a location where the circumstellar material is depleted and warm, appears indeed highly unlikely. Planet migration from further away distances where solid material is abundant, triggered by gravitational interactions, is invoked to account for this population. The exact process is still under debate but two major mechanisms are put forward: gradual planet migration due to interaction with the circumstellar gas disk (Lin et al., 1996; Papaloizou et al., 2007) or planet-planet or planet-companion star interactions combined with tidal dissipation (Rasio & Ford, 1996; Fabrycky & Tremaine, 2007; Nagasawa et al., 2008, e.g.). Whatever the exact nature of the formation path, these planets have undergone a significant orbital evolution since the time of their formation. Their current properties provide valuable hints helping to better understand their orbital evolution, especially the planet's orbit eccentricity and spin-orbit alignment of the system.

Up to now, transit surveys have been more sensitive to planets at very short orbital period. The situation has recently started to change thanks to the extended temporal coverage of ground-based transit surveys and the advent of space missions, *CoRoT* (Baglin et al., 2009; Deleuil et al., 2011) and Kepler (Borucki et al., 2010). As a consequence, the number of planets with orbital periods greater than a few days has significantly increased over the past two years. While the mean eccentricity for the close-in planets is close to zero, the transiting giant planets at larger orbital distance display a much wider range in eccentricity, a picture more consistent with the sample of planets found by radial velocity surveys. These trends favor a third body induced migration with tidal circularization of an initial eccentric and possibly high-obliquity orbit (Winn et al., 2010; Matsumura et al., 2010; Pont et al., 2011, e.g.). A consequence of this orbital evolution is the tidal destruction of the planet which spirals down onto the star in the life time of the system (Gonzalez, 1997; Jackson et al., 2009), a dramatic destruction that appears being the fate of the vast majority of the transiting planets (Matsumura et al., 2010).

In this paper, we report on the discovery of *CoRoT-20b*, a new member of the hot-Jupiter class population. The planet transits its G-type parent star every 9.24 days, along an orbit with a high eccentricity. The *CoRoT* observations are presented in Section 2. The accompanying follow-up observations and their results are described in Section 3 and Section 5 for the host-star

<sup>★</sup> The CoRoT space mission, launched on December 27th 2006, has been developed and is operated by CNES, with the contribution of Austria, Belgium, Brazil, ESA (RSSD and Science Programme), Germany and Spain.

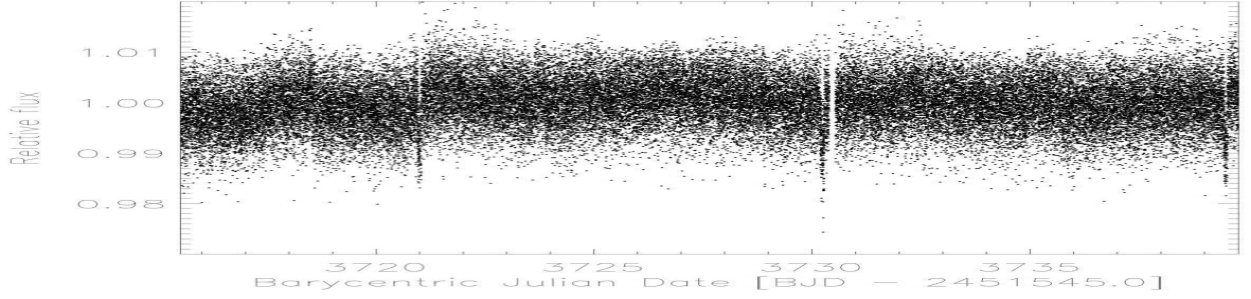


**Fig. 1.** The 24.278-days long *CoRoT-20* reduced light curve at a constant 512-sec time sampling.

analysis. The final system parameters are derived in Section 4. We then discuss the properties of this new planet in Section 6. We investigate its orbital evolution and fate but also its internal structure that rises new questions on the nature of such compact object.

## 2. *CoRoT-20b* Light curve

The planet has been discovered in one of the fields observed by the *CoRoT* satellite (Baglin et al., 2009; Deleuil et al., 2011) in the so-called *anti-center* direction. This field, labeled as *SRa03*, was monitored for 24.278 days starting on 1 March 2010. As a consequence of the DPU1 break down that took place on March 2009, the number of targets actually photometrically monitored by the instrument was reduced to a maximum of 6000 stars only. The released telemetry is further used to oversample a much larger number of targets than it was initially possible, up to magnitude  $\approx 15$ . While not among the brightest stars of the field (Table 1), *CoRoT-20* benefited this new opportunity and its observation was performed with the regular 32 sec time sampling. It was also bright enough to allow for three-color photometry. Two transits were detected in its light curve by the *Alarm mode* pipeline (Surace et al., 2008). The target was flagged as a good planetary candidate and put among the highest priorities for follow-up observations.

**Table 1.** *CoRoT-20b* IDs, coordinates and magnitudes.

CoRoT window ID	SRa03_E2_0999	
CoRoT ID	315239728	
USNO-B1 ID	0902-0091920	
2MASS ID	06305289+0013369	
GSC2.3 ID		
Coordinates		
RA (J2000)	97.720434	
Dec (J2000)	0.22692	
Magnitudes		
Filter	Mag	Error
B <sup>a</sup>	15.31	
V <sup>a</sup>	14.66	
J <sup>b</sup>	12.991	0.023
H <sup>b</sup>	12.652	0.026
K <sup>b</sup>	12.512	0.027

<sup>a</sup> from USNO-B1 - Provided by Exo-Dat (Deleuil et al., 2009);

<sup>b</sup> from 2-MASS catalog.

The light curve of *CoRoT-20b* is displayed in Fig 1. It shows a star rather quiet photometrically speaking, with no special prominent feature. Three transits are clearly visible with a period of 9.24 days and a depth slightly shallower than 1%. For the detailed analysis, we used the light curve reduced by the *CoRoT* calibration pipeline. It corrects for the main instrumental effects such as the CCD zero offset and gain, the background light and the spacecraft jitter (see Auvergne et al., 2009). Portions of the light curve that were flagged by the pipeline as affected by particle impacts during the South Atlantic Anomaly crossing, were removed and ignored in the analysis. In total, the light curve consists of 56869 photometric measurements. It gives a corresponding duty cycle of 88%.

## 3. Follow-up observations

A photometric time-series of the star was obtained at the Wise observatory on November 14, 2010 in order to check whether an unknown nearby eclipsing binary could be the source of the transits (Deeg et al., 2009). The detection of a transit ingress excluded this configuration at the spatial resolution of Wise. The observed time of the ingress, with first contact at  $2455515.510 \pm 0.007$  HJD was then used to refine the period of *CoRoT-20b*, towards the value quoted in Table 3. Ground-based images from both Wise and the DSS show that the star is rather isolated (Fig 2). This supports the very low contamination rate that was derived for the star within the CoRoT photometric mask (see Sec 4).

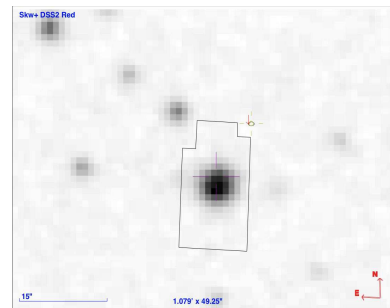


**Fig. 2.** Image of the DSS showing *CoRoT-20* and its environment. The photometric mask used for *CoRoT* observations is overplotted on the target.

Radial velocity (RV) observations started during the same season on December 9, 2010. We used the *HARPS* spectrograph (Mayor et al., 2003) mounted on the 3.6-m ESO tele-

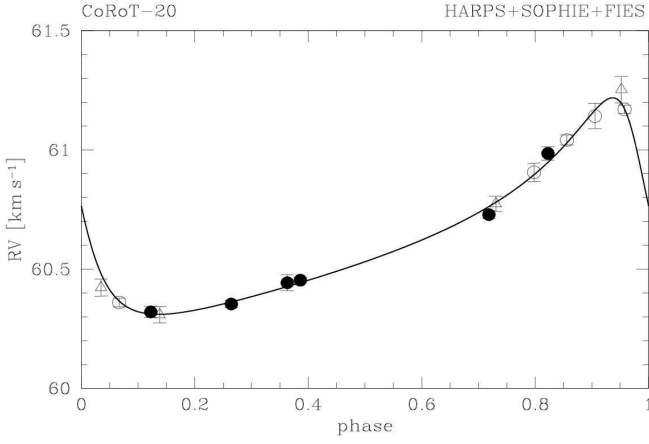


**Fig. 3.** The phase-folded radial velocity measurements of *CoRoT-20*. The various symbols correspond to the different spectrographs used for the follow-up campaign: *HARPS* (black circle), *SOPHIE* (open circle) and *FIES* (open triangle). The best fit solution is over-plotted in full line

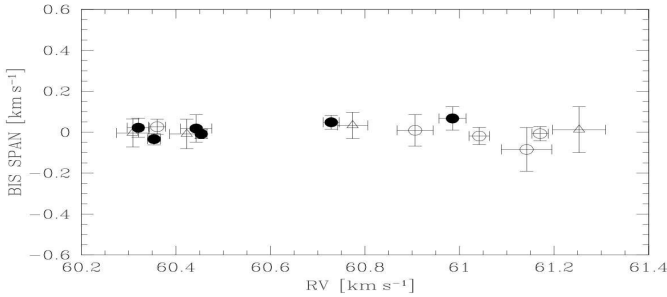


**Fig. 4.** Bisector span versus radial velocity of *CoRoT-20* showing no correlation.

scope (Chile) as part of the ESO large program 184.C-0639, the *SOPHIE* spectrograph (Perruchot et al., 2008) on the 1.93-m telescope at the Observatoire de Haute Provence (France) and the *FIES* spectrograph on the Nordic Optical Telescope (Frandsen & Lindberg, 1999) based on the 2.56-m Nordic Optical telescope in La Palma (Spain) under observing program P42-216.

We used the same instrument set-up as for previous *CoRoT* candidates follow-up : high resolution mode for *HARPS* and high efficiency mode for *SOPHIE* without acquisition of the simultaneous thorium-argon calibration, the second fiber being used to monitor the Moon background light (Santerne et al., 2011). For *HARPS* and *SOPHIE*, the exposure time was set to 1 hour. We reduced data and computed RVs with the pipeline based on the weighted cross-correlation function (CCF) using a numerical G2 mask (Baranne et al., 1996; Pepe et al., 2002).

*FIES* observations were performed in high-resolution mode with the 1.3 arcsec fiber yielding a resolving power  $R \approx 67\,000$  and a spectral coverage from 3600 to 7400 Å. Three consecutive exposures of 1200 sec were obtained for each observation. Long-exposed ThAr spectra were acquired right before and after each science spectra set, as described in Buchhave et al. (2010). Standard IRAF routines were used to reduce, combine, and wavelength calibrate the nightly spectra. RV measurements were derived cross-correlating the science spectra with the spec-

**Table 2.** Log of radial velocity observations

Date	HJD	$v_{\text{rad}}$ km s <sup>-1</sup>	$\sigma v_{\text{rad}}$ km s <sup>-1</sup>	Spectrograph
2010-12-09	55540.70645	60.728	0.0169	<i>HARPS</i>
2010-12-14	55545.75533	60.353	0.0138	<i>HARPS</i>
2011-01-12	55574.60927	60.453	0.0119	<i>HARPS</i>
2011-01-16	55578.64264	60.985	0.0285	<i>HARPS</i>
2011-01-21	55583.64035	60.443	0.0334	<i>HARPS</i>
2011-01-28	55590.66159	60.320	0.0234	<i>HARPS</i>
2011-01-16	55578.41934	60.813	0.0385	<i>SOPHIE</i>
2011-01-17	55579.41057	61.048	0.0532	<i>SOPHIE</i>
2011-02-04	55597.44200	60.948	0.0213	<i>SOPHIE</i>
2011-02-05	55598.38017	61.077	0.0175	<i>SOPHIE</i>
2011-02-06	55599.39134	60.267	0.0183	<i>SOPHIE</i>
2011-01-06	55568.55091	60.611	0.032	<i>FIES</i>
2011-01-08	55570.59973	61.090	0.060	<i>FIES</i>
2011-01-18	55580.60213	60.260	0.036	<i>FIES</i>
2011-01-19	55581.56506	60.146	0.034	<i>FIES</i>

trum of the RV standard star HD 50692 (Udry et al., 1999), observed with the same instrument set-up as *CoRoT-20*.

The 15 radial velocities of *CoRoT-20b* are listed in Table 2 and displayed in Fig. 3. They present a clear variation, in phase with the *CoRoT* ephemeris and consistent with a companion in the planet-mass regime with an eccentric orbit. We nevertheless investigated the possibility of an unresolved eclipsing binary being the source of observed transits. To that purpose, we performed the line-bisector analysis of the CCFs (see Fig. 4) and also checked that there is no dependency of the RVs variations with the cross-correlation masks constructed for different spectral types (Bouchy et al., 2009).

The Keplerian fit of the RVs was performed simultaneously with the transit modeling (see Section 4). All the parameters of the fit are listed in Table 3.

#### 4. System parameters

We calculated the flux contamination from nearby stars whose light might fall inside the *CoRoT* photometric mask using the same methodology as described in Bordé et al. (2010). The method takes into account the photometric mask used to perform the on-board photometry and all the stars in the target neighborhood, including faint background stars. We found the contamination being less than 0.6% and we further neglected it.

Three sections of the light curve, each centered on a transit, were locally normalized by fitting a third-degree polynomial. Each section was a 5-hours interval before the transit ingress and after its egress. The detailed physical modeling of the system was performed by carrying out the transit modeling and the Keplerian fit of the radial velocity measurements simultaneously. For the transit fit we used the formalism of Giménez (2006, 2009). The fit implies twelve free parameters : the orbital period  $P$ , the transit epoch  $T_{\text{tr}}$ , the transit duration  $T_{14}$ , the ratio of the planet to stellar radii  $R_p/R_*$ , the inclination  $i$  between the orbital plane and the plane of the sky, the Lagrangian orbital elements  $h = e \sin \omega$  and  $k = e \cos \omega$ , where  $e$  is the eccentricity and  $\omega$  the argument of the periastron, the radial-velocity semi-amplitude  $K$ , the systemic velocity  $\gamma_{\text{rel}}$  and the two offsets between *SOPHIE* and *HARPS* radial velocities and *SOPHIE* and *FIES*. For the transit modeling, we used a limb-darkening quadratic law (Claret, 2003, 2004). The limb-darkening coefficients  $u_a$  and  $u_b$  were taken using the tabulated values for the

*CoRoT* bandpass from Sing (2010) for the atmospheric parameters  $T_{\text{eff}}$ ,  $\log g$  and metallicity derived for the central star (see sect. 5):  $u_a = 0.4262 \pm 0.0168$  and  $u_b = 0.2434 \pm 0.0108$ . The two corresponding non-linear limb-darkening coefficients are  $u_+ = u_a + u_b = 0.6696 \pm 0.0201$  and  $u_- = u_a - u_b = 0.1828 \pm 0.0201$ . We decided to keep these limb-darkening parameter values fixed in the transit fitting.

The fit was performed using the algorithm AMOEBA (Press et al., 1992). The initial values of the fitted parameters were changed with a Monte-Carlo method to find the global minimum of the  $\chi^2$ . The associated 1-sigma errors were then estimated using a bootstrap procedure described in details in Bouchy et al. (2011). In such a procedure the limb-darkening parameters were allowed to vary within their error bars related to the atmospheric parameter uncertainties. The final values of the fitted parameters and the subsequently derived system parameters are given in Table 3. Fig. 5 displays the best fit compared to the observed folded transit.

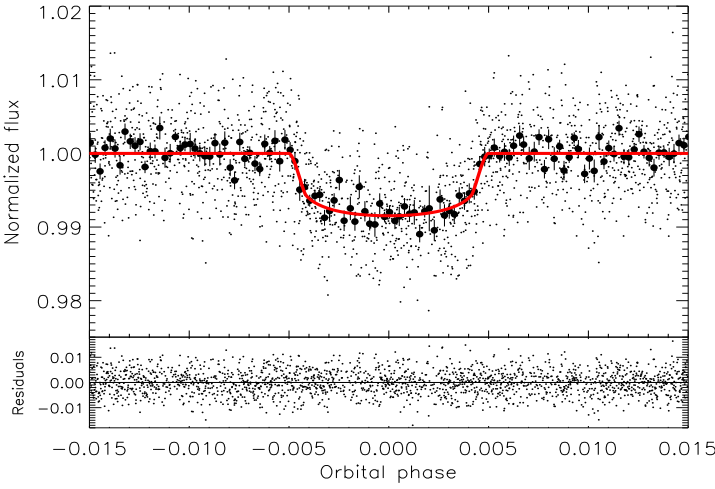


**Fig. 5.** The phase-folded transit in the phase space. The phase bins are 3.3 min and the error bar of each individual bin was calculated as the dispersion of the points inside the bin, divided by the square root of the number of points per bin. The best model is over plotted in full line.

## 5. Stellar parameters

The spectroscopic analysis was done the usual way it is carried out for the *CoRoT* planets: a master spectrum was created from the co-addition of spectra collected for the radial velocity measurements of the companion. We chose the *HARPS* spectra that offer the highest spectral resolution. We selected those that were not affected by the Moon reflected light at the time of the observations. Each order of the selected spectra was corrected by the blaze, set in the barycentric rest frame and rebinned to the same wavelength grid with a constant step of  $0.01\text{\AA}$ . The spectra were then co-added order per order. Each order of the co-added spectrum was then carefully normalized and the overlapping orders were merged resulting in a single 1D spectrum. This master spectrum has a S/N of 176 per element of resolution at  $5760\text{\AA}$  in the continuum.

A prior estimate of the atmospheric parameters  $T_{\text{eff}}$ ,  $\log g$ , chemical composition and  $v \sin i$  was performed by fitting the spectrum with a library of synthetic spectra calculated using

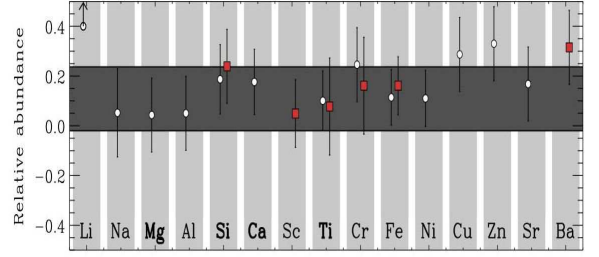


**Fig. 6.** Abundances of the chemical elements measured with VWA in the HARPS co-added spectrum of *CoRoT-20*. The abundances refer to the solar value. White circles correspond to neutral lines, red boxes to singly ionized lines and the yellow area represents the mean metallicity within one sigma error bar.

MARCS stellar atmosphere, including the  $H\alpha$  Balmer line. The rotational broadening was estimated on a selection of isolated spectral lines fitted by synthetic spectra convolved with various rotational velocities. We found  $v \sin i = 4.5 \pm 1.0 \text{ km s}^{-1}$  and  $v_{\text{macro}} = 3.5 \pm 1.0 \text{ km s}^{-1}$ . The detailed analysis was then carried out using the Versatile Wavelength Analysis package (VWA) (Bruntt et al., 2004, 2010b). A first set of weak and isolated lines of Fe I and Fe II was fitted until the derived abundances of Fe minimized the correlation with the equivalent width and the excitation potentials. We found:  $T_{\text{eff}} = 5880 \pm 90 \text{ K}$ ,  $\log g = 4.05 \pm 0.17$  and  $v_{\text{mic}} = 1.10 \pm 0.1 \text{ km s}^{-1}$  which corresponds to a G2-type dwarf. Then the abundances of other elements for which we could find isolated spectral lines were derived (see Fig 5). We performed an independent estimate of the surface gravity from the pressure-sensitive lines: the Mg I b lines, the Na I D doublet and the Ca I at  $6122\text{\AA}$  and  $6262\text{\AA}$ . We fitted the spectrum with the aforementioned grid of synthetic spectra in regions centered on each of the spectral lines of interest. The inferred value of the surface gravity is  $\log g = 4.2 \pm 0.15$ , a value in good agreement with the  $\log g$  derived with VWA obtained from the agreement between the Fe I and Fe II abundances. We thus adopted  $\log g = 4.2$  for the surface gravity.

The mean metallicity of the star is computed as the mean of metals with more than 10 lines in the spectrum, such as Si, Ca, Ti, Fe, Ni (Fig. 5). This yields a straight mean of  $[M/H] = 0.14 \pm 0.05$ . The error on  $[M/H]$  due to the uncertainty on  $T_{\text{eff}}$ ,  $\log g$  and microturbulence is 0.11 dex, which we must add quadratically to get  $[M/H] = 0.14 \pm 0.12$  (Bruntt et al., 2010a).

We also checked for any indicators of age. We found no hint of stellar activity in the Ca II H and K lines. However, the Li I line is clearly detected at  $6708\text{\AA}$  (see Fig. 7). We measured an equivalent width of  $W_{\text{eq}} = 44 \text{ m\AA}$  and determined a lithium abundance of 2.97. Following Sestito & Randich (2005), this leads to an age in the range 100 Myr up to 1 Gyr, depending on the star's initial rotation velocity.

The modeling of the star in the HR diagram was carried out in the  $(T_{\text{eff}}, M_{\star}^{1/3}/R_{\star})$  plane taking the host-star's metallicity into account. It resulted in the final estimates of the star's fundamental parameters given in Table 3:  $M_{\star} = 1.14 \pm 0.08 M_{\odot}$ ,  $R_{\star} = 1.02 \pm 0.05 R_{\odot}$ . The inferred surface gravity is  $\log g = 4.47 \pm 0.11$ , in agreement within the errors with the spectroscopic result. The evolutionary status points to a young star likely in the last stages of the pre-MS phase. We found the most likely isochrone age being  $100^{+800}_{-40} \text{ Myr}$ , a result in good agreement with the Li abundance.



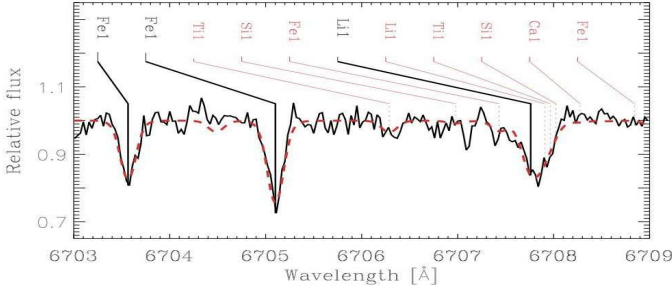


**Fig. 7.** *CoRoT-20* spectrum in a spectral region around the Li I lines at 6708 Å.

We calculated the distance of the star. We used the parameters of the star we derived and its 2-*MASS* magnitudes to estimate the reddening. We found a color excess  $E(J-K) = 0.18$  mag and the absorption  $A_V = 1.04 \pm 0.5$  mag using the extinction law from Schlegel et al. (1998). This yields a distance of  $1.23 \pm 0.12$  kpc, consistent with the strong interstellar absorption observed in the Na I (D1) and (D2) lines.

## 6. CoRoT-20 system properties

Compared to the sample of known transiting planets, *CoRoT-20b* is unusual in many respect. With an orbital period of 9.24 days it joins the group of transiting planets with periods outside the pile-up at 3 days. It is the fifth planet discovered by *CoRoT* in this period domain which currently accounts for 25 planets (see <http://exoplanet.eu/>), 9 out of these belonging to multi-planet systems : Kepler-9 (Holman et al., 2010), Kepler-10 (Fressin et al., 2011) and Kepler-11 (Lissauer et al., 2011). However all these Kepler-planets have a mass which is less than  $\sim 0.3 M_{\text{Jup}}$  and could not be directly compared to the giant planet population. Excluding these planets in multiple systems, for the 17 remaining objects of the sample that do not have a detected companion, 8, that is 47%, have a significant eccentric orbit with  $e$  in the range 0.15 to 0.9.

Planets with highly eccentric orbit appear to be found preferentially among the high-mass and/or long period planet population. With a mass of  $4.13 M_{\text{Jup}}$  which places it at the border of the gap in mass between the regular hot-Jupiter population and the very massive planet one, *CoRoT-20b* is consistent this trend. In the mass-period diagram they are clearly separated from the lighter planets with circular orbits (Pont et al., 2011). This dichotomy and in particular the lack of massive close-in planets at circular orbit suggest that tidal evolution should play an important role in the fate of the planet population.

### 6.1. Tidal evolution

Following Levrard et al. (2009) approach we checked the stability of *CoRoT-20b* to tidal dissipation. The authors calculated the ratio between the total angular momentum of a given system  $L_{\text{tot}}$  and the critical angular momentum  $L_{\text{crit}}$  for some transiting systems. According to Hut (1980), tidal equilibrium states exist when the total angular momentum is larger than this critical value  $L_{\text{crit}}$ . However, this equilibrium state could be stable or unstable, depending whether the orbital angular momentum  $L_{\text{orb}}$  is more than three time the total spin angular momentum  $L_{\text{spin}}$ , or not. Levrard et al. (2009) demonstrated that for none of the systems but HAT-P-2b the stable tidal equilibrium state, that corresponds to  $L_{\text{tot}}/L_{\text{crit}} > 1$ , exists. Further the fate of these

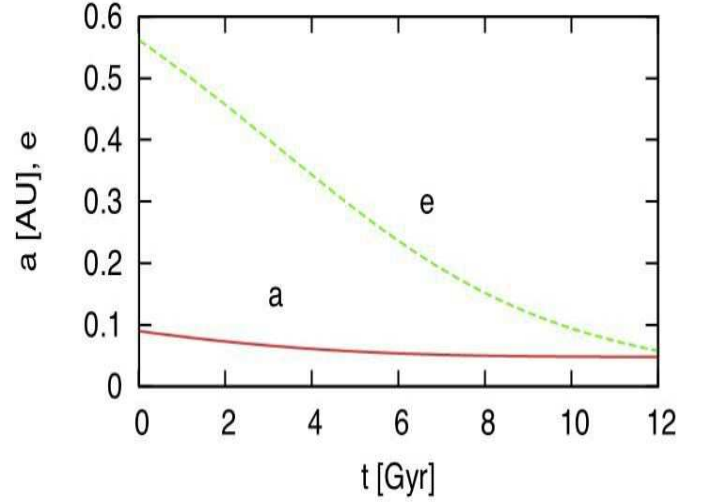


**Fig. 8.** Tidal evolution of the orbital semi-major axis and eccentricity. The figure is displayed on a time interval larger than the expected lifetime of the star to show the triple synchronization characteristic of a Darwin-stable system.

close-in planets is ultimately a collision with their host-star. The study has been recently reexamined and extended to more than 60 transiting systems by Matsumura et al. (2010) who achieved a similar conclusion, showing that the vast majority of these close-in planets will spiral-in to their host star and will be destroyed by tides. Using equations (1) and (2) given by Levrard et al. (2009) that neglect any effect of a possible magnetized stellar wind, we found for *CoRoT-20b*:

$$L_{\text{tot}}/L_{\text{crit}} = 1.057 \quad \text{and} \quad L_{\text{spin}\star}/L_{\text{orb}} = 0.0458$$

It shows that, within the current observational uncertainties, the planet has a tidal equilibrium state. It is worth noticing that our approach also assumes the stellar obliquity is small. The later is poorly constrained as the star's rotation period could not be derived from the light curve. We simply assumed that the rotation axis is perpendicular to the line of sight and derived the star's rotation period from the  $v \sin i$  (Table 3), a regular method for transiting systems. This gives a rotational period of the star of  $11.5 \pm 3.1$  days, that is of the same order than the planet's orbital period. In the case of *CoRoT-20b*,  $L_{\text{spin}\star}/L_{\text{orb}} < 1/3$  and most of the angular momentum of the system is in the orbit. According to Matsumura et al. (2010), *CoRoT-20b* belongs to the very small subgroup of Darwin-stable systems that evolve toward a stable tidal equilibrium state where migration will stop.

From the Roche-limit separation, the planet thus lies well beyond two times the Roche limit distance. Using (Faber et al., 2005) :

$$a_R = (R_p/0.462)(M_\star/M_p)^{1/3}$$

we found that the Roche limit  $a_R$  of the system is 0.0057 AU. This further supports the migration scenario over the scattering/Kozai-cycle scenario as proposed by Ford & Rasio (2006).

We performed a complete calculation of the tidal evolution of the system formed by the star and the planet assuming a linear tidal model (Mignard, 1979; Hut, 1981). The main difficulty here is to choose the values of the dissipation in the star and in the planet. For the main semi-diurnal tides of the star, we have adopted the value  $Q'_s = 10^7$  as found for hot Jupiters (Hansen, 2010; Benítez-Llambay et al., 2011). Because of the

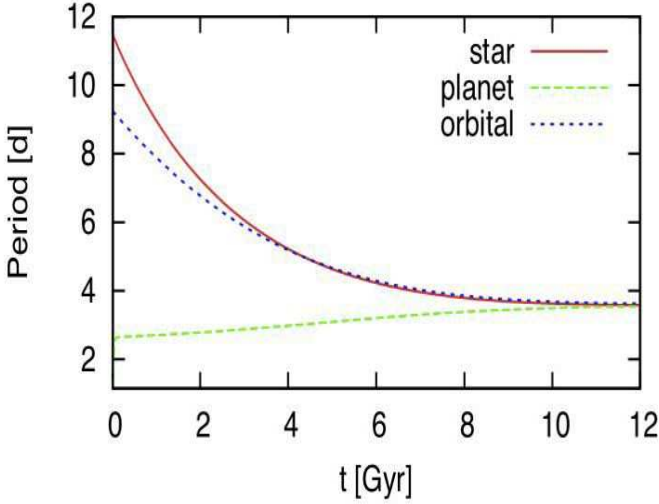


Fig. 9. Tidal evolution of the rotational and orbital periods.

close values of the orbital period and the rotation of the star, the components of the tides raised on the star by the planet related to the orbital eccentricity are also equally important, but the values of the current dissipation obtained with them are of the same order of magnitude. For the planet, we have derived one value on the basis of the actually determined  $Q'$  of Jupiter ( $Q' = 1.36 \times 10^5$ , see Lainey et al. (2009)). We first note that standard linear tidal theories (see Hut, 1981, eqn 45) allow us to determine the current rotation period (stationary) of the planet independently of the dissipation. We obtain  $2.64 \pm 0.13$  days. To transform  $Q'_{\text{Jup}}$  into the planet's  $Q'_p$ , we have to take into account: (i)  $Q'_p$  scales with the semi-diurnal tide period (see Ferraz-Mello et al., 2008; Matsumura et al., 2010); (ii)  $Q'_p$  scales with  $R_p^{-5}$  (see Eggleton et al., 1998; Ogilvie & Lin, 2004). We thus obtain  $Q'_p = 2.2 \times 10^6$ . Fig. 8 shows the variation of the semi-major axis and the evolution of the eccentricity. One can notice that with the adopted dissipation values, while the eccentricity tends toward zero, the circularization will not be achieved within the lifetime of the system.

Fig. 9 shows the evolution of the periods. The planet rotation is currently in a stationary super-synchronous state, that is the planet rotation is faster than its orbital motion. Its period increases as the eccentricity decreases and almost synchronization is reached when the eccentricity becomes very small. The star rotation period is currently decreasing; it will equal the synchronous value at some time 4 Gyr from now. However, it will continue to decrease up to reach the triple synchronous stationary state. The triple synchronization, however, does not seem to be reached within the lifetime of the star.

It is worth underlining that the actual  $Q'$  values are not known and the values we used are only estimates founded on previous studies. Therefore the exact timescale of the tidal processes is uncertain. Furthermore, by extracting angular momentum from the system, stellar magnetic braking may prevent the planet from reaching a triple synchronous state and ultimately jeopardize its survival (Bouchy et al., 2011). Indeed, simulations in which magnetic braking was active during the whole system lifetime, following the model proposed by (Bouvier et al., 1997) and using the same tide parameters as in the examples given above, show that the planet is falling below the Roche limit in about 6 Gyr. This result is critically dependent on the adopted

parameters and further would require a detailed study that is well beyond the scope of the present paper.

We also investigate the consequences of the circularization of the planet orbit which is in the phase of fast circularization, on the transits occurrence. Assuming there is no other close massive perturber in the system, then two effects are causing TTVs: the decrease of the orbital semi-major axis and the circularization of the orbit. Concerning the orbital semi-major axis, the time-scale of its variation,  $\dot{a}$ , is  $-0.9510^{-5}$  1/Myr presently (see Fig 9). As a consequence, a continuous period variation of  $\dot{P}/P \approx -410^{-12}$  per cycle is expected. As well-known, this linear period variation will cause a parabolic  $O-C$  curve, and in 100 years from now the  $O-C$  value will be only  $-25$  seconds. This is slightly over the  $3\sigma$  observation limit by *CoRoT* (Bean, 2009; Csizmadia et al., 2010). Assuming that the transit timing precision can be forced down to 5 sec in the future, this  $O-C$  value will be reached in 45 years from now.

Turning to the evolution of the eccentricity during the circularization process, it has two consequences. First the occurrence of the secondary eclipse will change. The displacement  $D$  of the secondary from phase 0.5 is given by (eqn 1 and 2 Borkovits, 2004, e.g.). The previous results of the tidal evolution calculations indicated  $\dot{e} = -4.5 \cdot 10^{-5}$  1/Myr and  $\dot{P} = -1.5 \cdot 10^{-3}$  days/Myr. Assuming a constant  $\omega$ , we have that  $\dot{D} = -37.56 \cdot 10^{-5}$  days/Myr or  $\dot{D} = -9.53 \cdot 10^{-12}$  days/cycle. This variation is of the same order as the previous one caused by the decreasing semi-major axis, so it would be observable within a century, too.

For the second effect, that is the circularization of the orbit, one can also consider the occurrence of a small precession of the orbit. This effect is hardly observable, but interesting on the theoretical side, since the transit occurs at the true anomaly  $v = 90^\circ - \omega$  where  $\omega$  is the argument of periastrion. The later is also subject to variations because of theory of general relativity but also because the tidal effects force the apsidal line to rotate. However, this variation has a different time-scale. We thus do not take this into account here, even if tidal forces also cause a small precession of the orbit showing that  $\dot{\omega}$  is not zero. So if  $e$  decreases due to circularization, and even if  $\omega$  is constant, then at the epoch of transit the eccentric anomaly will increase and hence the mean anomaly at transit will occur later. However, a first estimation shows that this effect may be negligible in a ten year timescale.

## 6.2. Internal structure

*CoRoT-20b* is a massive hot-Jupiter with a mass of  $4.24 M_{\text{Jup}}$  a radius of  $0.84 M_{\text{Jup}}$ , and an inferred density  $\rho = 8.87 \pm 1.1 \text{ g cm}^{-3}$ . A few giant planets are already reported with similar density or even higher : *CoRoT-14b*  $\rho = 7.3 \pm 1.5 \text{ g cm}^{-3}$  (Tingley et al., 2011), *WASP-18b*  $\rho = 8.8 \pm 0.9$  (Hellier et al., 2009; Southworth, 2010) or *HAT-P-20b*  $\rho = 13.78 \pm 1.5 \text{ g cm}^{-3}$  (Bakos et al., 2010) for example. While the mass of these planets spans a large range, from  $\sim 4$  up to more than  $9 M_{\text{Jup}}$ , their radius is close to  $1 R_{\text{Jup}}$ . Given *CoRoT-20b*'s large planetary mass, its small size is surprising. Among these high density giants planets, only *HAT-P-20b* has a comparable size, i.e.  $0.867 \pm 0.033 R_{\text{Jup}}$ . *CoRoT-20b*, as *HAT-P-20b*, is thus expected to contain large amounts of heavy elements in its interior.

To investigate the internal structure of *CoRoT-20b*, we computed planetary evolution models with CEPAM (Guillot & Morel, 1995), following the description in Guillot & Havel (2011), and Havel et al. (2011) for a planet of

a total mass  $4.24 M_{\text{Jup}}$ . We derived a time-averaged equilibrium temperature of the planet to be  $T_{\text{eq}} = 1002 \pm 24$  K. The results for  $T_{\text{eq}} = 1000$  K are shown in Fig. 10 in terms of the planetary size as a function of the system age. The coloured regions (green, blue, yellow) indicate the constraints derived from the CESAM stellar evolution models (Morel & Lebreton, 2008) at 1, 2, and  $3\sigma$  level, respectively. For preferred ages between 100 Ma and 1 Ga, we find that *CoRoT-20b* should contain between 680 and  $1040 M_{\oplus}$  of heavy-elements in its interior (i.e. between 50 and 77% of the total planetary mass), at  $1\sigma$  level, about twice the amount needed for HAT-P-20b (see Leconte et al., 2011). While this result is qualitatively in line with the observed correlation between star metallicity and heavy elements in the planet (e.g. Guillot et al., 2006; Miller & Fortney, 2011, and references therein), the derived amounts are extremely surprising. They would imply that all the heavy elements of a putative gaseous protoplanetary disk of 0.1 to  $0.15 M_{\odot}$  were filtered out to form *CoRoT-20b*, and then that an extremely small fraction of hydrogen and helium in that disk was accreted by the planet. This is at odds with today's accretion formation models (e.g. Ida & Lin, 2004; Mordasini et al., 2009). Disk instability with differentiation and partial tidal stripping (Boley & Durisen, 2010) is proposed as an alternative formation pathway. According to Boley et al. (2011), this could account for giant planets with massive core such as HAT-P-20b. In its current orbit, *CoRoT-20b* doesn't enter the Roche limit and no tidal stripping is acting on yet but this scenario would deserve further investigations.

We investigated the possibility that changes in the atmospheric model would yield more "reasonable" values for the planetary enrichment. As can be seen from a similar study in the brown dwarf regime (Burrows et al., 2011), the consequences of modified atmospheric properties are limited for objects with the mass of *CoRoT-20b* (i.e. standard radii for objects of this mass range from  $1.05$  to  $1.20 R_{\text{Jup}}$ ). By artificially lowering the infrared atmospheric opacity by a factor 1000 (not shown), we were able to decrease the  $1\sigma$  upper limit to the core mass from  $650$  to  $390 M_{\oplus}$ , a small change compared to huge and unphysical decrease in the opacity.

On the other hand, one strong assumption in our study is that heavy elements are embedded into a central core. When relatively small amounts of heavy elements are considered, it is not very important whether they are considered as being part of a core or mixed in the envelope (e.g. Ikoma et al., 2006). However, as shown by Baraffe et al. (2008), when  $0.5 M_{\text{Jup}}$  of ices are mixed in the envelope of a  $1 M_{\text{Jup}}$  planet, its radius is smaller by  $\sim 0.1 R_{\text{Jup}}$  than when one considers that these elements are part of a central core. It is thus very likely that the mass of heavy elements required to explain the radius of *CoRoT-20b* is high but significantly smaller than considered here. Estimates based on the Baraffe et al. (2008) calculations indicate that if mixed in the envelope, a mass of heavy elements 2 to 3 times smaller than estimated in Fig. 10 would explain the observed planetary size. This would alleviate the problem of the formation of the planet, although it would still require relatively extreme/unlikely scenarios.

## 7. Summary

In this article we presented the discovery of *CoRoT-20b*. The object belongs to the population of massive planets with orbital semi major axes below 0.1 AU, a domain of orbital periods where low and high eccentricity systems co-exist in a narrow range of orbital period. We examined the tidal stability of

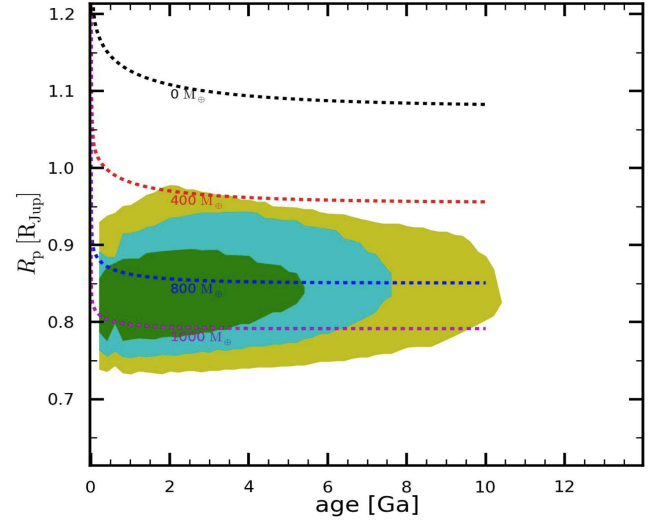


**Fig. 10.** Evolution of the size of *CoRoT-20b* (in Jupiter units) as a function of age (in billion years), compared to constraints inferred from *CoRoT* photometry, spectroscopy, radial velocimetry and stellar evolution models. Green, blue and yellow regions correspond to the planetary radii and ages that result from stellar evolution models matching the inferred  $\rho_{\star} - T_{\text{eff}} - [\text{Fe}/\text{H}]$  uncertainty ellipse within  $1\sigma$ ,  $2\sigma$  and  $3\sigma$ , respectively. Planetary evolution models for a planet with a solar-composition envelope over a central dense core of variable mass (0, 400, 800, and  $1000 M_{\oplus}$  as labelled) are shown as dashed lines. These models also assume that 1% of the incoming stellar irradiation is dissipated deep into the interior of the planet.

*CoRoT-20* and found that, within the observational uncertainties, it belongs to the relatively small population of transiting planets that are considered as "Darwin-stable", i.e. systems for which in the absence of processes extracting angular momentum from the system (i.e. stellar winds), the planet would never fall onto the central star which would instead be spun-up towards triple-synchronization (equality of the orbital, planetary and stellar spin periods). Other cases in the planetary domain are *CoRoT-3b*, *CoRoT-6b*, WASP-7 and HD 80606 (Matsumura et al., 2010). Measuring the stellar obliquity through the Rossiter-McLaughlin effect would provide additional constraints to better constrain its tidal evolution and further understand its orbital evolution. The expected semi-amplitude of the radial velocity anomaly of the Rossiter-McLaughlin effect is estimated to be  $22 \pm 5 \text{ m s}^{-1}$ , unfortunately quite difficult to detect with the present spectrographs used for the keplerian orbit determination. Another point would be to assess the presence of any additional companions in the system by long-term radial velocity monitoring as, according to Matsumura et al. (2010), the formation path of close-in planet should be different for single-planet system and multi-planet ones. *CoRoT-20* system appears thus an interesting bench test case to study the tidal orbital and rotational evolution of the close-in population.

The second interesting peculiarity that distinguishes *CoRoT-20b* from the regular giant planet population is its small observed radius. According to planetary evolution models, the interior of this compact planet should contain a very high amount of heavy elements, with a central dense core whose mass would be in the range between 680 and  $1040 M_{\oplus}$ . Although mixing heavy elements in the envelopes rather than confining them to a central core can lead to substantially smaller values (by a factor esti-

mated to be  $\sim 2 - 3$ ), the origin of such a huge amount of heavy elements is difficult to explain within the framework provided by the current planetary formation models. With HAT-P-20b (Bakos et al., 2010), it is the second example of extremely metal rich interior that challenges planetary interior models. However, the two planetary systems differ in many aspects: HAT-P-20 mass is nearly twice that of *CoRoT-20b*; it orbits on a nearly circular orbit a K3 metal rich star, while *CoRoT-20* is a solar-type, slightly metal enriched star. In addition, HAT-P-20 seems to be physically associated to another stellar companion, while up to now, *CoRoT-20* has none, detected or suspected. It thus appears difficult from this two exceptions to derive any trend that would provide hints on the origin these challenging and intriguing bodies.

**Acknowledgements.** The French team thanks the CNES for its continuous support to the *CoRoT/Exoplanet* program. The authors wish to thank the staff at ESO La Silla Observatory for their support and for their contribution to the success of the HARPS project and operation. The team at the IAC acknowledges support by grants ESP2007-65480-C02-02 and AYA2010-20982-C02-02 of the Spanish Ministry of Science and Innovation (MICINN). The *CoRoT/Exoplanet* catalogue (Exodat) was made possible by observations collected for years at the Isaac Newton Telescope (INT), operated on the island of La Palma by the Isaac Newton group in the Spanish Observatorio del Roque de Los Muchachos of the Instituto de Astrofísica de Canarias. The German *CoRoT* team (TLS and University of Cologne) acknowledges DLR grants 500W0204, 500W0603, and 50QP0701. The Swiss team acknowledges the ESA PRODEX program and the Swiss National Science Foundation for their continuous support on *CoRoT* ground follow-up. A. S. Bonomo acknowledges CNRS/CNES grant 07/0879-Corot. S. Aigrain acknowledges STFC grant ST/G002266. M. Gillon acknowledges support from the Belgian Science Policy Office in the form of a Return Grant.

## References

- Auvergne, M., Bodin, P., Boissard, L., et al. 2009, *A&A*, 506, 411  
 Baglin, A., Auvergne, M., Barge, P., et al. 2009, in *IAU Symposium*, Vol. 253, IAU Symposium, 71–81  
 Bakos, G. Á., Hartman, J., Torres, G., et al. 2010, *ArXiv e-prints*  
 Baraffe, I., Chabrier, G., & Barman, T. 2008, *A&A*, 482, 315  
 Baranne, A., Queloz, D., Mayor, M., et al. 1996, *A&AS*, 119, 373  
 Bean, J. L. 2009, *A&A*, 506, 369  
 Benítez-Llambay, P., Masset, F., & Beaugé, C. 2011, *A&A*, 528, A2+  
 Boley, A. C. & Durisen, R. H. 2010, *ApJ*, 724, 618  
 Boley, A. C., Helled, R., & Payne, M. J. 2011, *ApJ*, 735, 30  
 Bordé, P., Bouchy, F., Deleuil, M., et al. 2010, *A&A*, 520, A66+  
 Borkovits, T. 2004, *Publications of the Astronomy Department of the Eotvos Lorand University*, 14, 207  
 Borucki, W. J., Koch, D., Basri, G., et al. 2010, *Science*, 327, 977  
 Bouchy, F., Bonomo, A. S., Santerne, A., et al. 2011, *A&A*, 533, A83+  
 Bouchy, F., Moutou, C., Queloz, D., & the *CoRoT Exoplanet Science Team*. 2009, in *IAU Symposium*, Vol. 253, IAU Symposium, 129–139  
 Bouvier, J., Forestini, M., & Allain, S. 1997, *A&A*, 326, 1023  
 Bruntt, H., Bedding, T. R., Quirion, P., et al. 2010a, *MNRAS*, 405, 1907  
 Bruntt, H., Bikmaev, I. F., Catala, C., et al. 2004, *A&A*, 425, 683  
 Bruntt, H., Deleuil, M., Fridlund, M., et al. 2010b, *A&A*, 519, A51+  
 Buchhave, L. A., Bakos, G. Á., Hartman, J. D., et al. 2010, *ApJ*, 720, 1118  
 Burrows, A., Heng, K., & Nampaisarn, T. 2011, *ArXiv e-prints*  
 Claret, A. 2003, *A&A*, 401, 657  
 Claret, A. 2004, *A&A*, 428, 1001  
 Csizmadia, S., Renner, S., Barge, P., et al. 2010, *A&A*, 510, A94+  
 Deeg, H. J., Gillon, M., Shporer, A., et al. 2009, *A&A*, 506, 343  
 Deleuil, M., Meunier, J. C., Moutou, C., et al. 2009, *AJ*, 138, 649  
 Deleuil, M., Moutou, C., & Bordé, P. 2011, *Detection and Dynamics of Transiting Exoplanets*, St. Michel l’Observatoire, France, Edited by F. Bouchy; R. Díaz; C. Moutou; EPJ Web of Conferences, Volume 11, id.01001, 11, 1001  
 Eggleton, P. P., Kiseleva, L. G., & Hut, P. 1998, *ApJ*, 499, 853  
 Faber, J. A., Rasio, F. A., & Willems, B. 2005, *Icarus*, 175, 248  
 Fabrycky, D. & Tremaine, S. 2007, *ApJ*, 669, 1298  
 Ferraz-Mello, S., Rodríguez, A., & Hussmann, H. 2008, *Celestial Mechanics and Dynamical Astronomy*, 101, 171  
 Ford, E. B. & Rasio, F. A. 2006, *ApJ*, 638, L45  
 Frandsen, S. & Lindberg, B. 1999, in *Astrophysics with the NOT*, ed. H. Karttunen & V. Pirola, 71–+  
 Fressin, F., Torres, G., Desert, J.-M., et al. 2011, *ArXiv e-prints*  
 Giménez, A. 2006, *A&A*, 450, 1231  
 Giménez, A. 2009, in *Astronomical Society of the Pacific Conference Series*, Vol. 404, The Eighth Pacific Rim Conference on Stellar Astrophysics: A Tribute to Kam-Ching Leung, ed. S. J. Murphy & M. S. Bessell, 291–+  
 Gonzalez, G. 1997, *MNRAS*, 285, 403  
 Guillot, T. & Havel, M. 2011, *A&A*, 527, A20+  
 Guillot, T. & Morel, P. 1995, *A&AS*, 109, 109  
 Guillot, T., Santos, N. C., Pont, F., et al. 2006, *A&A*, 453, L21  
 Hansen, B. M. S. 2010, *ApJ*, 723, 285  
 Havel, M., Guillot, T., Valencia, D., & Crida, A. 2011, *A&A*, 531, A3+  
 Hellier, C., Anderson, D. R., Collier Cameron, A., et al. 2009, *Nature*, 460, 1098  
 Holman, M. J., Fabrycky, D. C., Ragozzine, D., et al. 2010, *Science*, 330, 51  
 Hut, P. 1980, *A&A*, 92, 167  
 Hut, P. 1981, *A&A*, 99, 126  
 Ida, S. & Lin, D. N. C. 2004, *ApJ*, 616, 567  
 Ikoma, M., Guillot, T., Genda, H., Tanigawa, T., & Ida, S. 2006, *ApJ*, 650, 1150



- Jackson, B., Barnes, R., & Greenberg, R. 2009, *ApJ*, 698, 1357
- Lainey, V., Arlot, J.-E., Karatekin, Ö., & van Hoolst, T. 2009, *Nature*, 459, 957
- Leconte, J., Chabrier, G., Baraffe, I., & Levrard, B. 2011, *Detection and Dynamics of Transiting Exoplanets*, St. Michel l'Observatoire, France, Edited by F. Bouchy; R. Díaz; C. Moutou; EPJ Web of Conferences, Volume 11, id.03004, 110, 3004
- Levrard, B., Winisdoerffer, C., & Chabrier, G. 2009, *ApJ*, 692, L9
- Lin, D. N. C., Bodenheimer, P., & Richardson, D. C. 1996, *Nature*, 380, 606
- Lissauer, J. J., Fabrycky, D. C., Ford, E. B., et al. 2011, *Nature*, 470, 53
- Matsumura, S., Peale, S. J., & Rasio, F. A. 2010, *ApJ*, 725, 1995
- Mayor, M., Pepe, F., Queloz, D., et al. 2003, *The Messenger*, 114, 20
- Mignard, F. 1979, *Moon and Planets*, 20, 301
- Miller, N. & Fortney, J. J. 2011, *ArXiv e-prints*
- Mordasini, C., Alibert, Y., Benz, W., & Naef, D. 2009, *A&A*, 501, 1161
- Morel, P. & Lebreton, Y. 2008, *Ap&SS*, 316, 61
- Nagasawa, M., Ida, S., & Bessho, T. 2008, *ApJ*, 678, 498
- Ogilvie, G. I. & Lin, D. N. C. 2004, *ApJ*, 610, 477
- Papaloizou, J. C. B., Nelson, R. P., Kley, W., Masset, F. S., & Artymowicz, P. 2007, *Protostars and Planets V*, 655
- Pepe, F., Mayor, M., Galland, F., et al. 2002, *A&A*, 388, 632
- Perruchot, S., Kohler, D., Bouchy, F., et al. 2008, in *Presented at the Society of Photo-Optical Instrumentation Engineers (SPIE) Conference*, Vol. 7014, *Society of Photo-Optical Instrumentation Engineers (SPIE) Conference Series*
- Pont, F., Husnoo, N., Mazeh, T., & Fabrycky, D. 2011, *MNRAS*, 378
- Press, W. H., Teukolsky, S. A., Vetterling, W. T., & Flannery, B. P. 1992, *Numerical recipes in FORTRAN. The art of scientific computing*
- Rasio, F. A. & Ford, E. B. 1996, *Science*, 274, 954
- Santerne, A., Endl, M., Hatzes, A., et al. 2011, *Detection and Dynamics of Transiting Exoplanets*, St. Michel l'Observatoire, France, Edited by F. Bouchy; R. Díaz; C. Moutou; EPJ Web of Conferences, Volume 11, id.02001, 11, 2001
- Schlegel, D. J., Finkbeiner, D. P., & Davis, M. 1998, *ApJ*, 500, 525
- Sestito, P. & Randich, S. 2005, *A&A*, 442, 615
- Sing, D. K. 2010, *A&A*, 510, A21+
- Southworth, J. 2010, *MNRAS*, 408, 1689
- Surace, C., Alonso, R., Barge, P., et al. 2008, in *Presented at the Society of Photo-Optical Instrumentation Engineers (SPIE) Conference*, Vol. 7019, *Society of Photo-Optical Instrumentation Engineers (SPIE) Conference Series*
- Tingley, B., Endl, M., Gazzano, J.-C., et al. 2011, *A&A*, 528, A97+
- Udry, S., Mayor, M., & Queloz, D. 1999, in *Astronomical Society of the Pacific Conference Series*, Vol. 185, *IAU Colloq. 170: Precise Stellar Radial Velocities*, ed. J. B. Hearnshaw & C. D. Scarfe, 367–+
- Winn, J. N., Fabrycky, D., Albrecht, S., & Johnson, J. A. 2010, *ApJ*, 718, L145

**Table 3.** Planet and star parameters.

<i>Ephemeris</i>		
Planet orbital period $P$ [days]	$9.24285 \pm 0.00030$	<sup>1</sup> Laboratoire d'Astrophysique de Marseille, 38 rue Frédéric Joliot-Curie, 13388 Marseille cedex 13, France
Primary transit epoch $T_{tr}$ [BJD-2400000]	$55\,266.0001 \pm 0.0014$	<sup>2</sup> LESIA, Obs de Paris, Place J. Janssen, 92195 Meudon cedex, France
Primary transit duration $T_{14}$ [d]	$0.0927 \pm 0.0019$	<sup>3</sup> Institut d'Astrophysique Spatiale, Université Paris XI, F-91405 Orsay, France
Secondary transit epoch $T_s$ [BJD-2400000]	$55\,272.46 \pm 0.13$	<sup>4</sup> Observatoire de Haute Provence, 04670 Saint Michel l'Observatoire, France
<i>System parameters</i>		
Periastron epoch $T_{peri}$ [BJD-2400000]	55265.79074	<sup>5</sup> Institut d'Astrophysique de Paris, 98bis boulevard Arago, 75014 Paris, France
$e \sin \omega$	$0.468 \pm 0.017$	<sup>6</sup> Department of Physics, Denys Wilkinson Building Keble Road, Oxford, OX1 3RH
$e \cos \omega$	$0.312 \pm 0.022$	<sup>7</sup> Instituto de Astrofísica de Canarias, E-38205 La Laguna, Tenerife, Spain
Orbital eccentricity $e$	$0.562 \pm 0.013$	<sup>8</sup> Universidad de La Laguna, Dept. de Astrofísica, E-38200 La Laguna, Tenerife, Spain
Argument of periastron $\omega$ [deg]	$56.3^{+2.4}_{-2.3}$	<sup>9</sup> University of Vienna, Institute of Astronomy, Türkenschanzstr. 17, A-1180 Vienna, Austria
Radial velocity semi-amplitude $K$ [m s <sup>-1</sup> ]	$454 \pm 9$	<sup>10</sup> Institute of Planetary Research, German Aerospace Center, Rutherfordstrasse 2, 12489 Berlin, Germany
Systemic velocity $\gamma_{rel}$ [km s <sup>-1</sup> ]	$60.623 \pm 0.006$	<sup>11</sup> IAG, Universidade de Sao Paulo, Brazil
HARPS-SOPHIE offset velocity $V_{r1}$ [m s <sup>-1</sup> ]	$93 \pm 11$	<sup>12</sup> Research and Scientific Support Department, ESTEC/ESA, PO Box 299, 2200 AG Noordwijk, The Netherlands
SOPHIE-FIES offset velocity $V_{r2}$ [m s <sup>-1</sup> ]	$163 \pm 20$	<sup>13</sup> University of Liège, Allée du 6 août 17, Sart Tilman, Liège 1, Belgium
O-C residuals [m s <sup>-1</sup> ]	27	<sup>14</sup> Thüringer Landessternwarte, Sternwarte 5, Tautenburg 5, D-07778 Tautenburg, Germany
<i>Spectroscopic parameters</i>		
Effective temperature $T_{eff}$ [K]	$5880 \pm 90$	<sup>15</sup> Space Research Institute, Austrian Academy of Science, Schmiedlstr. 6, A-8042 Graz, Austria
Surface gravity $\log g$ [dex]	$4.20 \pm 0.15$	<sup>16</sup> School of Physics and Astronomy, Raymond and Beverly Sackler Faculty of Exact Sciences, Tel Aviv University, Tel Aviv, Israel
Metallicity [Fe/H] [dex]	$0.14 \pm 0.12$	<sup>17</sup> Observatoire de l'Université de Genève, 51 chemin des Maillettes, 1290 Sauverny, Switzerland
Stellar rotational velocity $v \sin i$ [km s <sup>-1</sup> ]	$4.5 \pm 1.0$	<sup>18</sup> Observatoire de la Côte d'Azur, Laboratoire Cassiopée, BP 4229, 06304 Nice Cedex 4, France
Spectral type	G2 V	<sup>19</sup> LUTH, Observatoire de Paris, CNRS, Université Paris Diderot; 5 place Jules Janssen, 92195 Meudon, France
<i>Stellar and planetary physical parameters from combined analysis</i>		
Star mass [ $M_\odot$ ]	$1.14 \pm 0.08$	<sup>20</sup> Department of Physics and Astronomy, Aarhus University, 8000 Aarhus C, Denmark
Star radius [ $R_\odot$ ]	$1.02 \pm 0.05$	<sup>21</sup> Wise Observatory, Tel Aviv University, Tel Aviv 69978, Israel
Distance of the system [kpc]	$1.23 \pm 120$	
Age of the star $t$ [Myr]	$100^{+800}_{-40}$	
Orbital semi-major axis $a$ [AU]	$0.0902 \pm 0.0021$	
Orbital distance at periastron $a_{per}$ [AU]	$0.0392 \pm 0.0017$	
Orbital distance at apastron $a_{apo}$ [AU]	$0.1409 \pm 0.0037$	
Planet mass $M_p$ [ $M_J$ ] <sup>c</sup>	$4.24 \pm 0.23$	
Planet radius $R_p$ [ $R_J$ ] <sup>c</sup>	$0.84 \pm 0.04$	
Planet density $\rho_p$ [ $g\,cm^{-3}$ ]	$8.87 \pm 1.10$	
Equilibrium temperature <sup>d</sup> $T_{eq}$ [K]	$1002 \pm 24$	
Equilibrium temperature at periastron <sup>d</sup> $T_{eq}^{per}$ [K]	$1444^{+53}_{-46}$	
Equilibrium temperature at apastron <sup>d</sup> $T_{eq}^{apo}$ [K]	$764 \pm 18$	

<sup>a</sup>  $a/R_\star = \frac{1+e \cos \nu_1}{1-e^2} \cdot \frac{1+k}{\sqrt{1-\cos^2(\nu_1+\omega-\frac{\pi}{2})\sin^2 i}}$ , where  $\nu_1$  is the true anomaly measured from the periastron passage at the first contact (see Giménez, 2009).

<sup>b</sup>  $b = \frac{a \cos i}{R_\star} \cdot \frac{1-e^2}{1+e \sin \omega}$

<sup>c</sup> Radius and mass of Jupiter taken as 71492 km and  $1.8986 \times 10^{30}$  g, respectively.

<sup>d</sup> zero albedo equilibrium temperature for an isotropic planetary emission.